

Sound velocities and single-crystal elasticity of orthoenstatite to 1073 K at ambient pressure

Jennifer M. Jackson^{*,1}, Stanislav V. Sinogeikin², Jay D. Bass

Department of Geology, University of Illinois, Urbana, IL 61801, USA

Received 15 March 2006; received in revised form 12 October 2006; accepted 10 November 2006

Abstract

Single-crystal Brillouin spectroscopy measurements have been carried out to 1073 K and ambient pressure to determine the elastic modulus tensor of a natural orthopyroxene, nearly pure Mg end-member ($\text{Mg}_{0.994}\text{Fe}_{0.002}\text{Al}_{0.004}$)₂($\text{Si}_{0.996}\text{Al}_{0.004}$)₂O₆ orthoenstatite. Three single-crystal specimens with orthogonal crystallographic orientations were prepared for Brillouin measurements to determine all the single-crystal elastic moduli (C_{ij}). The single-crystal elastic moduli were calculated using the measured velocities of sound and our independent measurement of the volume thermal expansion. These are, to our knowledge, the highest temperatures at which the complete single-crystal elastic modulus tensor of orthoenstatite has been measured. The elastic moduli at ambient conditions obtained in this study are in excellent agreement with previous measurements on Mg₂Si₂O₆ orthoenstatite (OEN). The elastic anisotropy of OEN is approximately the same at all measured temperatures. The velocities in different directions change at different rates, with C_{33} showing the largest temperature dependence (decreasing with temperature almost twice as fast as C_{11} or C_{22}). The variation of elastic moduli with temperature is linear up to approximately 673 K, above which some of the moduli decrease with a quadratic dependence on temperature. The non-linear behavior is in accord with recent elastic mode softening observations in orthoenstatite at higher temperatures and could add support to account for a thermally induced solid-state mechanism for the low velocity zone in Earth's upper mantle.

© 2007 Published by Elsevier B.V.

Keywords: Enstatite; High-temperature; Sound velocities; Elasticity; Brillouin spectroscopy

1. Introduction

Modeling the composition of Earth's upper mantle requires the comparison of geophysical observations, such as seismic data, with accurate determinations of

the sound velocities and elasticity of upper mantle minerals at appropriate pressure–temperature conditions. The major minerals in the upper mantle above about 300 km depth are olivine (ol), garnet (gt), orthopyroxene (opx), and clinopyroxene (cpx), with the volumetric proportions of these minerals depending on the mineralogical model used. The piclogite model suggests a comparatively low olivine content of about 40%, sub-equal proportions of garnet and Ca-cpx and a lesser amount of opx (Bass and Anderson, 1984; Duffy and Anderson, 1989), whereas, the pyrolite model suggests, approximately: ol = 60%, gt = 15%, cpx = 15%, opx = 10% (Ringwood, 1991). The obvious differences

* Corresponding author. Tel.: +1 626 395 6780.

E-mail address: jackson@gps.caltech.edu (J.M. Jackson).

¹ Current address: Geological and Planetary Sciences, California Institute of Technology, Pasadena, CA 91125, USA.

² Current address: HPCAT, Geophysical Laboratory, Carnegie Institution of Washington, Bldg. 434E, 9700 S. Cass Ave., Argonne, IL 60439, USA.

in mineralogical models are the olivine and garnet + Ca-cpx fractions, whereas, the proportion of opx is similar for each model. Orthopyroxene is also a major component (up to ~40%, e.g., Winter, 2001) in harzburgite, thereby making opx a major component in subducting oceanic slabs. At depths between ~300 km and ~490 km in the mantle, pyroxenes dissolve into garnet and form a majorite-garnet solid solution (Takahashi and Ito, 1987; Ita and Stixrude, 1993). To date, olivine and garnet have received a large amount of attention in terms of elasticity measurements at elevated pressures and temperatures on upper mantle minerals (Isaak et al., 1992; Li et al., 1998; Chen et al., 1996; Zha et al., 1996; Sinogeikin and Bass, 2000). Garnet and majorite are thought to have small elastic anisotropy under the pressure and temperature conditions of the upper mantle (Isaak et al., 1992; Parise et al., 1996; Pacalo and Weidner, 1997; Jiang et al., 2004; Sinogeikin and Bass, 2000, 2002a,b). Orthopyroxene, with a simplified formula of $(\text{Mg,Fe})_2\text{Si}_2\text{O}_6$ is also an abundant mineral in the upper mantle, being found primarily in mafic rocks of the crust and upper mantle (Deer et al., 1978). Therefore, knowledge of the sound velocities and elastic anisotropy of orthopyroxene under appropriate conditions is necessary to make accurate interpretations of seismic signatures in the upper mantle.

Brillouin scattering measurements (Weidner et al., 1978; Duffy and Vaughan, 1988; Jackson et al., 1999) and ultrasonic measurements (Kumazawa, 1969; Frisillo and Barsch, 1972; Weidner et al., 1978; Webb and Jackson, 1993) have been performed under ambient conditions to determine the sound velocities and single-crystal elasticity of the orthopyroxene: $(\text{Mg,Fe})_2\text{Si}_2\text{O}_6$ orthoenstatite. Several experiments have been performed to determine the elasticity of orthoenstatite at elevated pressures (Frisillo and Barsch, 1972; Dietrich and Arndt, 1982; Webb and Jackson, 1993; Angel and Hugh-Jones, 1994; Hugh-Jones and Angel, 1994; Flesch et al., 1998; Angel and Jackson, 2002; Kung et al., 2004; Nestola et al., 2006), but far fewer have been performed to determine the elasticity of orthoenstatite at elevated temperatures (Frisillo and Barsch, 1972; Zhao et al., 1995; Jackson et al., 2004). Only the high-pressure, high-temperature ultrasonic measurements by Frisillo and Barsch (1972) on $(\text{Mg}_{0.80}\text{Fe}_{0.20})_2\text{Si}_2\text{O}_6$ orthoenstatite could constrain the complete elastic tensor to 623 K and 1 GPa, and determined $(dK_S/dT)_P = -26.8 \text{ MPa/K}$ and $(d\mu/dT)_P = -11.9 \text{ MPa/K}$.

In a recent Brillouin scattering study to investigate the high-temperature phase transition of orthoenstatite, Jackson et al. (2004) report C_{33} and C_{55} to 1448 K. However, there are presently no experimental constraints on the temperature derivatives of the remaining single-

crystal moduli of orthoenstatite for appropriate mantle temperatures. This uncertainty affects modeling of the upper mantle. Furthermore, knowledge of the elastic properties of magnesium end-member orthoenstatite at mantle temperatures is important for assessing compositional variations amongst orthopyroxenes. In this study, we have determined the single crystal elastic moduli at high-temperatures for a natural orthoenstatite with a composition close to the Mg end-member. We show that orthoenstatite remains elastically anisotropic to the highest temperature reached in this study, namely 1073 K.

2. Experiment

Colorless, euhedral single crystals of orthoenstatite from Zabargad Island, Egypt (Kurat et al., 1993) were used in this study. These crystals are from the same batch as used in previous high-temperature Brillouin scattering (Jackson et al., 2004) and X-ray diffraction experiments (Jackson et al., 2003). Electron microprobe analyses were performed to determine the composition, $(\text{Mg}_{0.994}\text{Fe}_{0.002}\text{Al}_{0.004})_2(\text{Si}_{0.996}\text{Al}_{0.004})_2\text{O}_6$ (see Jackson et al., 2003). Polarized IR spectral analyses performed on Zabargad OEN from the same bulk sample indicates the presence of 70 wt. ppm OH^- (Skogby et al., 1990).

The Brillouin measurements were performed using an argon ion laser with an incident wavelength of $\lambda_0 = 514.5 \text{ nm}$. The scattered light was analyzed using a tandem 6-pass Fabry Perot interferometer (Sandercock, 1982) and a solid state detector (see Bass, 1989; Sinogeikin et al., 1998 for more details). The sound velocities were calculated from the measured frequency shifts using the following relationship for a symmetric scattering geometry (Whitfield et al., 1976):

$$V_i = \left(\frac{\lambda_0 \Delta \nu_{B,i}}{2 \sin(\theta^*/2)} \right) \quad (1)$$

where V_i is the quasi-compressional ($V_{i=P}$) or quasi-shear ($V_{i=S}$) phonon velocity, $\Delta \nu_{B,i}$ is the corresponding measured Brillouin shift, λ_0 is the incident argon ion laser wavelength ($\lambda_0 = 514.5 \text{ nm}$), and θ^* is the angle between the incident and the scattered light outside the sample or high-temperature cell (sometimes referred to as the external scattering angle). In the high-temperature measurements presented here, the scattering geometry was 80° . For measurements outside of the high-temperature cell at room-temperature, a 90° scattering geometry was used. All measurements were done at room-pressure.

Three single crystals with no visible inclusions were optically oriented and then polished with plane

normals to: [100], [010], and [001], and with a thickness of approximately 130 μm . X-ray diffraction verified the symmetry (*Pbca*) and orientation of the individual platelets before each Brillouin experiment. The platelet samples were first mounted on a glass fiber, outside the high-temperature cell for measurements under ambient conditions. The samples were then loaded into a high-temperature cell designed for platelet symmetric scattering and fixed into position using high-temperature zirconia cement (see Sinogeikin et al., 2000 for details of the high-temperature cell design). Room-temperature measurements were performed inside the high-temperature cell before increasing the temperature. In each high-temperature experiment, the temperature was first raised to 373 K and then increased by 100 K up to 1073 K. In this case, all three high-temperature experiments were performed under the same temperature conditions at ambient pressure. There was no reaction between the sample and cement during the temperature range of this study. The temperature was monitored using three thermocouples (two R-type and one K-type) positioned adjacent to the sample. The maximum temperature difference between

thermocouple readings was 5 K, and this occurred at 1073 K.

3. Room-temperature results

Typical Brillouin spectra at ambient conditions and at high-temperature are shown in Fig. 1. Combining measurements done inside and outside the high-temperature cell, Brillouin scattering spectra were collected in 51 distinct crystallographic directions under ambient conditions (over 300 data points; Fig. 2; filled symbols); both data sets are in excellent mutual agreement. In most directions, both the longitudinal and shear velocities were obtained. All of the data were collected within or very close to the (100), (010), and (001) crystallographic planes so that the on-diagonal elastic moduli are well constrained and independent of one another.

Orthoenstatite is orthorhombic and is therefore, characterized by nine independent single-crystal elas-

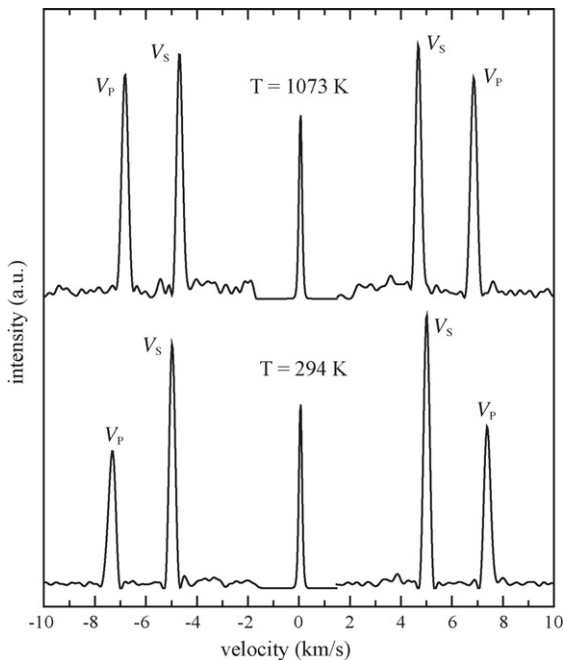


Fig. 1. Brillouin spectra for the same plane-normal [010] of orthoenstatite at 294 K and 1073 K inside the high-temperature cell at room-pressure. The peak at $V = 0$ km/s is the reference line and has been scaled down by five orders of magnitude. The velocity scale shown here has been converted from the measured spectrum (in GHz) using the relationship described in Eq. (1) for the scattering angle $\theta^* = 80^\circ$. The Brillouin scattered peaks for the windows of the high-temperature cell (zirconia) are outside the measured range shown here.

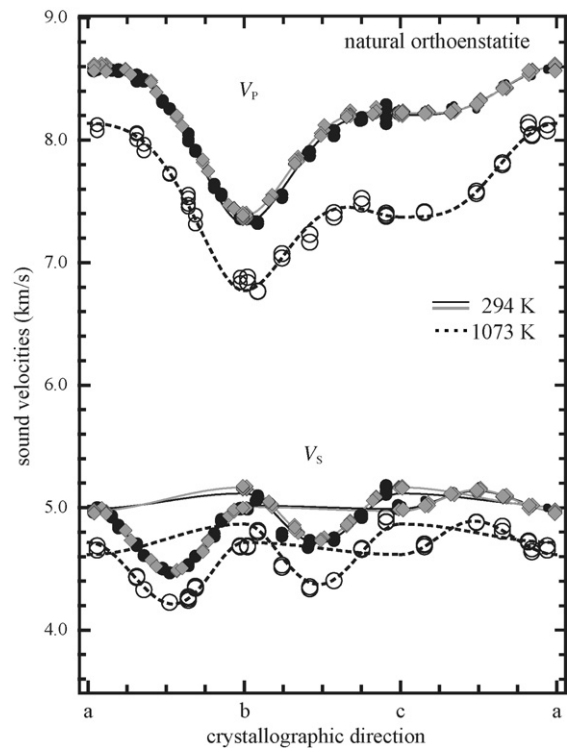


Fig. 2. Measured sound velocities of natural orthoenstatite as a function of crystallographic direction within the scattering planes (ab, [001]; bc, [100]; ac [010]) at room-temperature and 1073 K. The filled gray diamonds and filled black circles are measurements made outside the high-temperature cell and inside the cell, respectively, under ambient conditions. The open black circles are the data taken at 1073 K. The solid and dashed lines are calculated velocities from the best-fit single-crystal elastic moduli, as described in the text. All measurements were done at room-pressure.

tic moduli, C_{ij} (using reduced Voigt notation). The velocities of acoustic phonons are related to the single-crystal elastic moduli through the Christoffel equation (Musgrave, 1970):

$$\det|C_{ijkl}n_jn_l - \rho V^2\delta_{ik}| = 0 \quad (2)$$

where C_{ijkl} is the elastic modulus tensor, n_j and n_l are the unit vectors in the phonon propagation direction and the indices j and l are summed over, ρ is the density, V is phonon velocity, and δ_{ik} is the Kronecker delta. A linear inversion method described in Weidner and Carleton (1977) was used to calculate a best-fit model of the C_{ij} 's from the velocity data set, and the Voigt–Reuss–Hill averaging scheme was used to calculate the isotropic aggregate properties [adiabatic bulk modulus (K_S), shear modulus (μ), longitudinal velocity (V_P), and shear velocity (V_S)]. The C_{ij} 's, density, and isotropic aggregate properties for our room-temperature measurements are listed in Table 1, along with previous elasticity measurements on orthoenstatite.

The crystals investigated in this study are natural and very close to end-member $\text{Mg}_2\text{Si}_2\text{O}_6$ composition, with very minor amounts of aluminum and iron. It is, therefore, not surprising that the C_{ij} 's and isotropic aggregate properties obtained in this study are in very good agreement with two previous Brillouin measurements on synthetic $\text{Mg}_2\text{Si}_2\text{O}_6$ orthoenstatite (Weidner et al., 1978; Jackson et al., 1999). In a recent study, Angel and Jackson (2002) combined the results of four different experiments on $\text{Mg}_2\text{Si}_2\text{O}_6$ orthoenstatite (one Brillouin, one high-pressure ultrasonic, and two X-ray diffraction measurements) and obtained a best-fit value of $K_S = 106.8 \pm 0.5$ GPa, in agreement with the results presented here (Table 1). Ultrasonic measurements on sintered polycrystalline $\text{Mg}_2\text{Si}_2\text{O}_6$ orthoenstatite also show agreement (Flesch et al., 1998; Kung et al., 2004).

The elastic anisotropy of OEN is significant. If we express the elastic anisotropy as $A_i = (V_{i,\max} - V_{i,\min})/V_{i,\text{VRH}}$, then under ambient conditions, $A_P = 15\%$ and $A_S = 11\%$. The anisotropy in the compressional wave

Table 1
Room-temperature room-pressure elasticity of $\text{Mg}_2\text{Si}_2\text{O}_6$ orthoenstatite from single-crystal and polycrystalline adiabatic experiments

	This study ^{a,b}	Jackson et al. (1999) ^c	Weidner et al. (1978) ^c	Flesch et al. (1998) ^d	Kung et al. (2004) ^e
C_{11} (GPa)	236 (1)	233 (1)	224.7 (23)		
C_{22} (GPa)	173 (1)	171 (1)	177.9 (22)		
C_{33} (GPa)	216 (1)	216 (1)	213.6 (36)		
C_{44} (GPa)	84 (1)	83 (1)	77.6 (19)		
C_{55} (GPa)	79 (1)	79 (1)	75.9 (11)		
C_{66} (GPa)	80 (1)	77 (1)	81.6 (16)		
C_{12} (GPa)	74 (2)	73 (2)	72.4 (42)		
C_{13} (GPa)	57 (2)	56 (2)	54.1 (110)		
C_{23} (GPa)	50 (2)	50 (3)	52.7 (46)		
ρ (g/cm ³)	3.196 (4)	3.194 (6)	3.204	3.18 (3)	3.202
$K_{s,R}$ (GPa)	107.4 (15)	106.6 (10)	107		
$K_{s,V}$ (GPa)	109.5 (15)	108.6 (10)	108		
$K_{s,\text{VRH}}$ (GPa)	108.5 (15)	107.6 (15)	107.8	104 (2)	108.7 (37)
$\mu_{s,R}$ (GPa)	77.3 (7)	76.4 (7)	75		
$\mu_{s,V}$ (GPa)	78.6 (7)	77.2 (7)	76		
$\mu_{s,\text{VRH}}$ (GPa)	77.9 (7)	76.8 (7)	75.7	74.9 (15)	76.5 (5)
$V_{P,R}$ (km/s)	8.11 (8)	8.08	8.05		
$V_{P,V}$ (km/s)	8.19 (8)	8.14	8.09		
$V_{P,\text{VRH}}$ (km/s)	8.15 (8)	8.11	8.07	8.00	8.11
$V_{S,R}$ (km/s)	4.92 (5)	4.89	4.84		
$V_{S,V}$ (km/s)	4.96 (5)	4.92	4.87		
$V_{S,\text{VRH}}$ (km/s)	4.94 (5)	4.90	4.86	4.85	4.89

The isostress Reuss (R) and isostrain Voigt (V) bounds for the aggregate properties are given. The Voigt–Reuss–Hill (VRH) average (the arithmetic mean of the V and R bounds) is used to compare with polycrystalline studies. Reported uncertainties are given in parentheses for the last significant digit(s).

^a Measurements outside the high-temperature cell (shown as open diamonds in Figs. 3–6). These data are within the uncertainties of data obtained from room-temperature measurements inside the cell (see Table 2).

^b Natural single-crystal $(\text{Mg}_{0.994}\text{Fe}_{0.002}\text{Al}_{0.004})_2(\text{Si}_{0.996}\text{Al}_{0.004})_2\text{O}_6$.

^c Synthetic single-crystal $\text{Mg}_2\text{Si}_2\text{O}_6$ (synthesized by Ito, 1975).

^d Synthetic polycrystalline $\text{Mg}_2\text{Si}_2\text{O}_6$.

^e Synthetic polycrystalline $\text{Mg}_2\text{Si}_2\text{O}_6$. Elastic properties are from “X-ray data” in Kung et al. (2004); density, V_P , and V_S are calculated here from reported $V_0 = 832.918 \text{ \AA}^3$ (Kung et al., 2004).

velocity (V_P) results from the differences in elastic stiffness along the principal crystallographic directions. Specifically, the near Mg end-member natural orthoenstatite investigated here gives the following trend: C_{11} , $[100] > C_{33}$, $[001] > C_{22}$, $[010]$. This trend is characteristic of the $(\text{Mg,Fe})_2\text{Si}_2\text{O}_6$ enstatite-ferrosilite join at ambient conditions and has been extensively discussed in previous reports [see Bass and Weidner, 1984].

4. High-temperature results

At all elevated temperatures, Brillouin spectra were collected in roughly 20 distinct crystallographic directions (over 80 data points per temperature; Fig. 2; open symbols). An example of a Brillouin spectrum of orthoenstatite at 1073 K is shown in Fig. 1. At all temperatures investigated here, the trend of elastic moduli mentioned above remains the same, namely C_{11} , $[100] > C_{33}$, $[001] > C_{22}$, $[010]$. The same relationships were also found to hold for a natural single-crystal of $(\text{Mg}_{0.8}\text{Fe}_{0.2})_2\text{Si}_2\text{O}_6$ orthoenstatite investigated up to 623 K using ultrasonic methods (Frisillo and Barsch, 1972). At the highest temperature of this study, we find that the elastic anisotropy remains approximately the same as at room-temperature ($\Delta_P = 17\%$ and $\Delta_S = 10\%$).

In contrast, recent molecular dynamics simulations on $\text{Mg}_2\text{Si}_2\text{O}_6$ orthoenstatite at high-temperatures (Miyake and Kawano, 2005) did not observe anisotropy in V_S and underestimate V_P by $\sim 8\%$ and V_S by $\sim 15\%$ at room-temperature.

In order to calculate the single-crystal elastic moduli at high-temperatures, the density and, hence the thermal expansion must be known. In fact, the accuracy of high temperature elasticity results is directly linked to the accuracy with which the thermal expansion is known (Isaak et al., 1992; Li et al., 1998; Jackson et al., 2000). Jackson et al. (2003) reported high-temperature X-ray diffraction measurements on OEN from the same bulk sample used in this study and obtained the volume thermal expansion, α , that linearly increases with temperature: $\alpha(T) = 29.7(16) \times 10^{-6} \text{ K}^{-1} + 5.7(11) \times 10^{-9} \text{ K}^{-2}T$, in agreement with other investigations on orthoenstatite (Yang and Ghose, 1994; Hugh-Jones, 1997). Using the thermal expansion obtained by Jackson et al. (2003) to calculate the density at each appropriate temperature, the linear inversion method described in Weidner and Carleton (1977) was used to calculate the full elastic tensor at each temperature up to 1073 K (Table 2). The nine single crystal elastic moduli and their temperature depen-

Table 2

(a) Temperature (K), density (g/cm^3), and single-crystal elastic moduli (C_{ij}) (GPa) for natural orthoenstatite (this study) at room-pressure. The isostress Reuss and isostrain Voigt bounds for the aggregate properties derived from the single-crystal elasticity are given in (b); temperature (K), aggregate elastic moduli (GPa) and aggregate sound velocities (km/s). The uncertainties for all listed parameters at $T > 294$ K are on the order of 1.5%. Uncertainties in temperature never exceeded 5 K

T	ρ	C_{11}	C_{22}	C_{33}	C_{44}	C_{55}	C_{66}	C_{12}	C_{13}	C_{23}
294 ^a	3.196	236	173	216	84	79	80	74	57	50
294	3.196	236	171	215	84	80	80	73	56	49
373	3.188	233	170	212	83	79	78	72	53	48
473	3.178	231	167	205	81	78	78	71	53	46
573	3.167	227	162	200	80	75	76	69	50	45
673	3.157	222	158	195	79	74	76	67	49	43
773	3.146	219	156	189	78	72	73	65	46	42
873	3.135	216	152	183	76	72	72	64	44	40
973	3.125	211	150	177	76	69	69	63	41	38
1073	3.113	206	143	169	74	66	69	60	37	36

T	$K_S(\text{Reuss})$	$K_S(\text{Voigt})$	$\mu_S(\text{Reuss})$	$\mu_S(\text{Voigt})$	$V_P(\text{Reuss})$	$V_P(\text{Voigt})$	$V_S(\text{Reuss})$	$V_S(\text{Voigt})$
294 ^a	107.4	109.5	77.3	78.6	8.11	8.19	4.92	4.96
294	106.6	108.8	77.0	78.3	8.09	8.17	4.91	4.95
373	105.1	107.0	76.3	77.6	8.05	8.13	4.89	4.93
473	102.4	104.7	75.0	76.3	7.98	8.06	4.86	4.90
573	99.8	102.0	73.3	74.6	7.90	7.98	4.81	4.85
673	96.9	99.2	72.0	73.3	7.82	7.90	4.77	4.82
773	94.6	96.7	70.7	72.0	7.75	7.83	4.74	4.78
873	91.9	94.1	69.4	70.6	7.67	7.75	4.70	4.75
973	89.2	91.3	67.8	69.1	7.58	7.66	4.66	4.71
1073	84.8	87.0	66.1	67.5	7.45	7.54	4.61	4.65

^a Measurement outside the high-temperature cell.

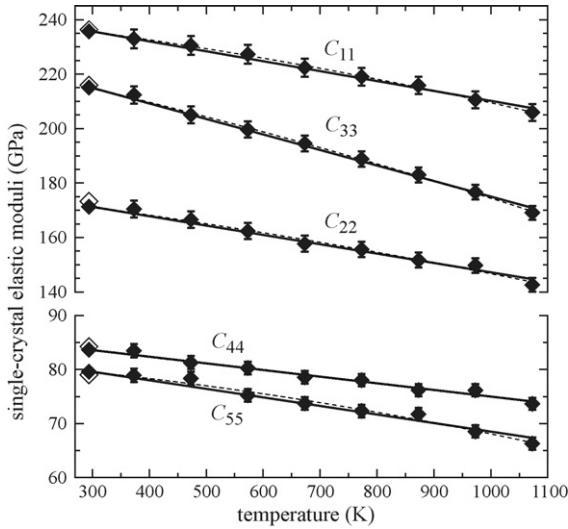


Fig. 3. The single-crystal elastic moduli (C_{11} – C_{55}) of orthoenstatite as a function of temperature at room-pressure. Open symbols are from data measured outside the high-temperature cell. The uncertainties at room-temperature are smaller than the symbol size. Solid and dashed lines are linear (Table 3) and second order polynomial (Table 4) fits to the elastic moduli with temperature, respectively, and were constrained to pass through the room-temperature values.

dependencies are plotted in Figs. 3 and 4. Isotropic aggregate properties at high-temperatures were calculated using the Voigt–Reuss–Hill averaging scheme and are plotted in Figs. 5 and 6. In Fig. 6, we also plot previous determinations of the elasticity of orthoenstatite. The uncertainties in the parameters at elevated temperatures

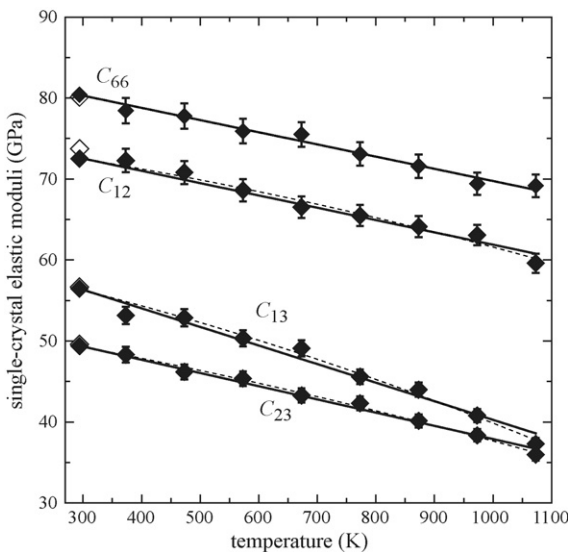


Fig. 4. The single-crystal elastic moduli (C_{66} , C_{12} , C_{13} , and C_{23}) of orthoenstatite as a function of temperature at room-pressure. Symbols and lines have the same meaning as in Fig. 3.

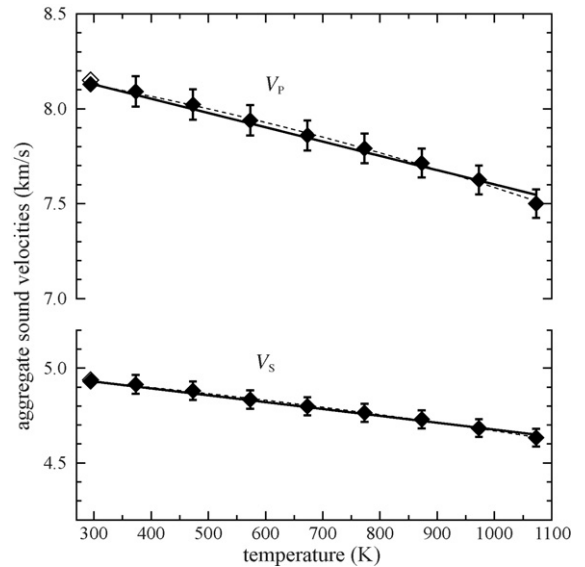


Fig. 5. Aggregate sound velocities (VRH) of orthoenstatite as a function of temperature. Symbols and lines have the same meaning as in Fig. 3.

are about 1.5%, which are higher than the uncertainties at room-temperature (<1%) due to the sampling statistics (see Fig. 2).

5. Discussion

Our high-temperature data are well explained by linear relations up to 1073 K (Figs. 3–6; Table 3), although some values are fit better to quadratic polynomial expressions. We therefore, provide quadratic polynomial expressions for our results (Table 4), because previous high-temperature Brillouin symmetric scattering measurements to 1448 K on one of the same single-crystals of orthoenstatite studied here (plane normal [0 1 0]) showed significant acoustic softening at $T > 973$ K (Jackson et al., 2004). We note that the linear and polynomial fits applied to our data (Tables 3 and 4, respectively) were constrained to pass through our room-temperature values. This constraint was used because the room-temperature values have lower uncertainties due to better angular sampling statistics (see Fig. 2). Although only a subset of crystallographic directions was sampled in Jackson et al. (2004), the elastic moduli C_{33} and C_{55} could be obtained up to 1448 K, with C_{33} showing the highest rate of softening with increasing temperature (these velocities are listed here in Table 5). The elastic moduli C_{33} and C_{55} obtained from an inversion of the data from three orthogonal crystallographic planes (this study) are in excellent agreement with those reported in Jackson et al. (2004) for the

Table 3

Linear temperature derivatives of the single-crystal elastic properties (MPa/K), aggregate VRH elastic properties (MPa/K) and aggregate VRH sound velocities (km/s) K⁻¹ of orthoenstatite and other upper mantle minerals

	Orthoenstatite			Diopside	Forsterite	Pyrope ^a
	This study	This study	Frisillo and Barsch (1972) ^b	Isaak et al. (2006) ^c	Suzuki et al. (1983) ^d	Suzuki and Anderson (1983)
<i>T</i> range (K) →	294–1073	294–573	298–623	298–1300	298–1200	298–1000
(∂ <i>C</i> ₁₁ /∂ <i>T</i>) _P	−36.4 (1)	−30.1 (1)	−35.3 (1)	−29.1	−38.4 (−40.1)	−36
(∂ <i>C</i> ₂₂ /∂ <i>T</i>) _P	−34.3 (1)	−29.7 (1)	−32.8 (1)	−24.8	−26.9 (−28.2)	−36
(∂ <i>C</i> ₃₃ /∂ <i>T</i>) _P	−57.0 (1)	−54.9 (1)	−51.6 (4)	−17.9	−29.4 (−32.1)	−36
(∂ <i>C</i> ₄₄ /∂ <i>T</i>) _P	−12.3 (1)	−12.0 (1)	−13.1 (2)	−10.3	−12.3 (−12.8)	−8.7
(∂ <i>C</i> ₅₅ /∂ <i>T</i>) _P	−15.8 (1)	−12.9 (1)	−13.8 (2)	−7.7	−12.5 (−13.3)	−8.7
(∂ <i>C</i> ₆₆ /∂ <i>T</i>) _P	−15.1 (1)	−16.1 (1)	−14.5 (5)	−15.2	−14.1 (−15.0)	−8.7
(∂ <i>C</i> ₁₂ /∂ <i>T</i>) _P	−15.2 (2)	−12.4 (2)	−21.2 (7)	−11.9	na	−11.1
(∂ <i>C</i> ₁₃ /∂ <i>T</i>) _P	−22.9 (2)	−22.2 (2)	−31.8 (8)	−6.4	na	−11.1
(∂ <i>C</i> ₂₃ /∂ <i>T</i>) _P	−16.3 (2)	−15.2 (2)	−10.7 (7)	0.0	na	−11.1
(∂ <i>K</i> _s /∂ <i>T</i>) _P	−26.3 (3) ^e	−23.8 (3)	−26.8	−12.3	−15.9 (−16.0)	−19.4
(∂ <i>μ</i> /∂ <i>T</i>) _P	−13.6 (3)	−12.5 (3)	−11.9	−9.98	−12.7 (−13.5)	−10.2
(∂ <i>V</i> _P /∂ <i>T</i>) _P (×10 ⁻⁴)	−7.53 (8)	−6.50 (8)	−9.08	−3.66	−4.9	na
(∂ <i>V</i> _S /∂ <i>T</i>) _P (×10 ⁻⁴)	−3.62 (5)	−3.17 (5)	−4.86	−2.56	−3.3	na

The linear fits listed below for this study were constrained to pass through the room-temperature values (see text). Reported uncertainties are given in parentheses for the last significant digit(s). na – not given in cited reference.

^a Natural pyrope: Py_{0.726}Alm_{0.157}Gr_{0.006}Sp_{0.007}And_{0.043}Uv_{0.061}.

^b Natural single-crystal (Mg_{0.8}Fe_{0.2})₂Si₂O₆ (Frisillo and Barsch, 1972).

^c Diopside is monoclinic and therefore needs four additional elastic moduli to describe its elastic variation with temperature, namely: (∂*C*₁₅/∂*T*)_P = 2.5, (∂*C*₂₅/∂*T*)_P = 2.2, (∂*C*₃₅/∂*T*)_P = −4.6, and (∂*C*₄₆/∂*T*)_P = 2.6 MPa/K (Isaak et al., 2006).

^d Values given and those in parenthesis are computed derivatives at 300 K and 1200 K, respectively (Suzuki et al., 1983).

^e Zhao et al. (1995) measured the thermoelasticity of Mg₂Si₂O₆ orthoenstatite at simultaneous high pressures (to 4.5 GPa) and temperatures (to 1000 K) and obtained (∂*K*_T/∂*T*)_P = −35 ± 5 (MPa/K), which converts to (∂*K*_S/∂*T*)_P = −27 ± 5 (MPa/K), using $\alpha(T) = 28.6(29) \times 10^{-6} \text{ K}^{-1} + 0.72(16) \times 10^{-9} \text{ K}^{-2} T$ and $\gamma = 1.05$ (Zhao et al., 1995) with the following expression: (∂*K*_S/∂*T*)_P = (∂*K*_T/∂*T*)_P + $\alpha\gamma T / (1 + \alpha\gamma T)$.

Table 4

Elasticity coefficients for a second order polynomial fit (this study)

<i>M</i> ₀	<i>M</i> ₁ ^a	<i>M</i> ₂ ^b
<i>C</i> ₁₁	−0.0285	−1.24 × 10 ⁻⁵
<i>C</i> ₂₂	−0.0287	−8.78 × 10 ⁻⁶
<i>C</i> ₃₃	−0.0503	−1.05 × 10 ⁻⁵
<i>C</i> ₄₄	−0.0122	−2.18 × 10 ⁻⁷
<i>C</i> ₅₅	−0.0111	−7.36 × 10 ⁻⁶
<i>C</i> ₆₆	−0.0153	3.11 × 10 ⁻⁷
<i>C</i> ₁₂	−0.0119	−5.18 × 10 ⁻⁶
<i>C</i> ₁₃	−0.0184	−7.05 × 10 ⁻⁶
<i>C</i> ₂₃	−0.0137	−4.05 × 10 ⁻⁶
<i>K</i> _{s,VRH}	−0.0217	−7.18 × 10 ⁻⁶
<i>μ</i> _{s,VRH}	−0.0119	−2.59 × 10 ⁻⁶
<i>V</i> _{P,VRH}	−5.71 × 10 ⁻⁴	−2.84 × 10 ⁻⁷
<i>V</i> _{S,VRH}	−2.88 × 10 ⁻⁴	−1.14 × 10 ⁻⁷

$M = M_0 + M_1(T - 294) + M_2(T - 294)^2$. The polynomial fits listed below for this study were constrained to pass through the room-temperature values (see text). The temperature is given in degrees Kelvin.

^a Units for the elasticity coefficients are (GPa/K) and for velocity coefficients are (km/s)K⁻¹.

^b Units for the elasticity coefficients are (GPa/K²) and for velocity coefficients are (km/s)K⁻².

temperature range in which these studies overlap (to 1073 K).

In a pressure–volume–temperature (*P*–*V*–*T*) experiment on a single-crystal of Mg₂Si₂O₆ orthoenstatite to 4.5 GPa and 1000 K, Zhao et al. (1995) used a modified Birch–Murnaghan equation of state at several temperatures to determine the thermal expansion (α), isothermal bulk modulus (*K*_{T0}), pressure derivative of the bulk modulus (*dK*_T/*dP*), and temperature derivative of the bulk modulus (*dK*_T/*dT*)_P. Zhao et al. determined that the best fit model to a combination of their data and previous compression and thermal expansion data gave (*dK*_T/*dT*)_P = −37 ± 5 MPa/K, a value that appears ~25% higher than that obtained in this study and by Frisillo and Barsch (1972) (Table 3). These differences can be reconciled using the adiabatic to isothermal conversion factor for these derivatives, namely (∂*K*_S/∂*T*)_P = (∂*K*_T/∂*T*)_P + $\alpha\gamma T / (1 + \alpha\gamma T)$. Therefore, (*dK*_T/*dT*)_P = −37 ± 5 MPa/K converts to (∂*K*_S/∂*T*)_P = −27 ± 5 MPa/K, using $\alpha(T) = 28.6(29) \times 10^{-6} \text{ K}^{-1} + 0.72(16) \times 10^{-9} \text{ K}^{-2} T$ and $\gamma = 1.05$ from Zhao et al. (1995). Although, the errors are large for the *P*–*V*–*T* results, the (∂*K*_S/∂*T*)_P values for

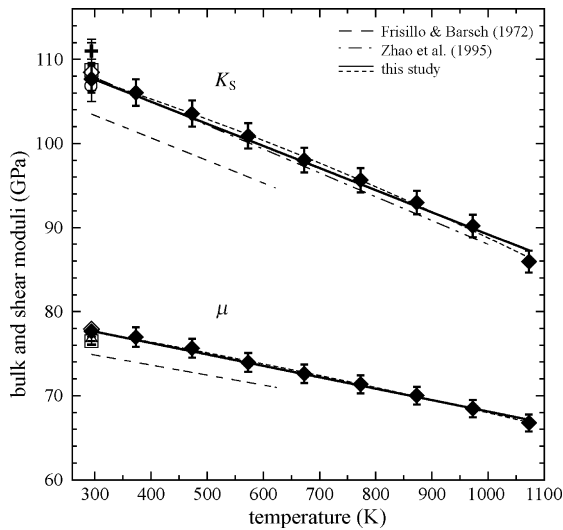


Fig. 6. Adiabatic bulk and shear elastic moduli (VRH) of orthoenstatite as a function of temperature at room-pressure. Symbols and lines have the same meaning as in Fig. 3. In addition, other elasticity measurements on orthoenstatite have been plotted. Adiabatic measurements—triangle: Jackson et al. (1999); square: Kung et al. (2004); long dashed line: Frisillo and Barsch (1972, natural $(\text{Mg}_{0.8}\text{Fe}_{0.2})_2\text{Si}_2\text{O}_6$ orthoenstatite). Combination of adiabatic and isothermal data—circle: Angel and Jackson (2000). The isothermal value of Nestola et al. (2006, cross, $\text{Ca}_{0.07}\text{Mg}_{1.93}\text{Si}_2\text{O}_6$ orthoenstatite) was corrected to an adiabatic value using the relation $K_S = K_T(1 + \alpha\gamma T)$, where $\gamma = 1.05$ (Zhao et al., 1995) and $\alpha(T) = 29.7 \times 10^{-6} + 5.7 \times 10^{-9} \text{K}^{-2}T$ (Jackson et al., 2003). The description of how the data of Zhao et al. (1995, dot-dashed line) was corrected to adiabatic values is in the text. All compositions are near Mg end-member $\text{Mg}_2\text{Si}_2\text{O}_6$ orthoenstatite, unless otherwise noted.

the Mg-end-member (Zhao et al., 1995 and this study) show good agreement for the effect of temperature on the bulk modulus of orthoenstatite (see Table 3). Note that iron does not have a significant effect on $(\partial K_S/\partial T)_P$, because, Frisillo and Barsch (1972) obtained $(\partial K_S/\partial T)_P = -26.8 \text{ MPa/K}$ for $(\text{Mg}_{0.8}\text{Fe}_{0.2})_2\text{Si}_2\text{O}_6$ orthoenstatite.

The role that crystal structure and/or iron incorporation play in determining the elastic properties of pyroxenes have been discussed previously (Frisillo and Barsch, 1972; Weidner and Vaughan, 1982; Vaughan and Bass, 1983; Weidner et al., 1982; Bass and Weidner, 1984; Duffy and Vaughan, 1988; Chai et al., 1997; Jackson et al., 1999). The only reported high-temperature investigation of the single-crystal elastic moduli of iron-bearing orthopyroxene is that of Frisillo and Barsch (1972), who performed measurements to 1 GPa and 623 K on four natural orthoenstatite samples of approximate composition $(\text{Mg}_{0.8}\text{Fe}_{0.2})_2\text{Si}_2\text{O}_6$ using the ultrasonic pulse superposition technique. Many linear temperature derivatives from our study (using

Table 5

Directional compressional (V_P) and shear (V_S) wave velocities in enstatite as a function of temperature for the crystallographic direction that shows the largest amount of softening [001] (from Jackson et al., 2004)

T	V_P	V_S
296	8.24	5.01
296	8.22	5.00
373	8.14	4.97
473	8.13	4.97
473	8.12	4.96
573	8.01	4.91
673	7.95	4.88
773	7.82	4.82
773	7.82	4.83
873	7.75	4.79
973	7.58	4.72
973	7.56	4.73
1073	7.42	4.67
1073	7.42	4.68
1073	7.43	4.69
1123	7.33	4.65
1148	7.29	4.64
1173	7.26	4.63
1198	7.12	4.58
1198	7.14	4.50
1223	7.07	4.56
1223	7.05	4.57
1248	6.96	4.54
1248	6.98	4.54
1273	6.90	4.52
1273	6.91	4.52
1298	6.78	4.49
1298	6.77	4.47
1323	6.69	4.46
1323	6.68	4.48
1348	6.52	4.42
1348	6.55	4.42
1373	6.38	4.38
1373	6.35	4.37
1398	6.10	4.31
1398	6.10	4.33
1423	5.82	4.25
1423	5.89	4.26
1448 ^a	7.30	4.88

At several temperatures multiple spectra were collected and the results are listed.

^a Structural phase transition has occurred to a high-temperature polymorph.

the entire temperature range, 294–1073 K) differ from the values obtained from these previous ultrasonic measurements (Table 3). In order to compare our study more directly with that of Frisillo and Barsch (1972), we also fit our elasticity data to a linear function in the temperature range of 294 to 573 K (Table 3). Simply by reducing the temperature range of the fit, one can see that the temperature derivatives

of most of the parameters increase (absolute values decrease) for orthoenstatite in our study. However, major differences still exist. We evaluated the choice of thermal expansion on the data; however, quantities such as the temperature derivatives of the aggregate sound velocities do not depend on density and therefore cannot be explained by the choice of the thermal expansion coefficients used. The study of Frisillo and Barsch (1972) used the thermal expansion of Frisillo and Buljan (1972), $\alpha = 47.7 \times 10^{-6} \text{ K}^{-1}$. We used $\alpha(T) = 29.7(16) \times 10^{-6} \text{ K}^{-1} + 5.7(11) \times 10^{-9} \text{ K}^{-2}T$ (Jackson et al., 2003), a value determined for powdered orthoenstatite from the same bulk sample as studied in the current study. If we used the thermal expansion given by Frisillo and Buljan (1972), a -1% difference in density at $\sim 600 \text{ K}$ results, and therefore, leads to a -10% difference in the temperature derivatives of the bulk and shear moduli. This difference is now too large to explain the differences in the temperature derivatives of the bulk and shear moduli (Table 3). We conclude that sample composition may play a major role in these differences.

Taking into account the entire data range of this study, the larger temperature derivatives for C_{33} in near Mg end-member orthoenstatite (this study) and iron-bearing orthoenstatite suggests that iron-bearing OEN may behave in a similar way as the Mg end-member in this particular crystallographic direction. The composition we investigated here undergoes a phase transition at higher temperatures that is accompanied by the softening of at least two elastic moduli (C_{33} and C_{55} , Jackson et al., 2004). The same type of mode-softening transition could occur in iron-bearing orthoenstatite with the same driving mechanism. However, the highest temperature obtained to determine the sound velocities of $(\text{Mg}_{0.8}\text{Fe}_{0.2})_2\text{Si}_2\text{O}_6$ orthoenstatite was only 623 K (Frisillo and Barsch, 1972). Therefore, any acoustic mode-softening due to a high-temperature transition in $(\text{Mg}_{0.8}\text{Fe}_{0.2})_2\text{Si}_2\text{O}_6$ orthoenstatite has yet to be detected. An indication that a structural phase transition would occur in iron-bearing orthoenstatite at high-temperatures and room-pressure is supported by X-ray diffraction measurements (Yang and Ghose, 1995a,b). In orthoenstatite there are two nonequivalent silicate chains known as A and B chains along [001] that are kinked at room-temperature (with the B chain being more kinked than the A chain) (Smyth, 1974a,b). At temperatures approaching the structural phase transition, the B chain shows a greater rate of straightening than the A chain until both chains become equivalent (Yang and Ghose, 1995a,b). Such a phenomenon has been suggested to be the driving mechanism for the

high-temperature low-pressure phase transition in iron-bearing orthoenstatite (Yang and Ghose, 1995b) and the Mg end-member (Yang and Ghose, 1995a; Jackson et al., 2004).

If we compare our data to recent ultrasonic measurements on Cr-bearing $\text{MgCaSi}_2\text{O}_6$ diopside (a clinopyroxene) (Isaak et al., 2006), we see that most of the temperature derivatives for enstatite are a lot higher than those for clinopyroxene and other upper mantle minerals (Table 3). Specifically, the measured value of $(dK_S/dT)_P = -23.8(3) \text{ MPa/K}$ for orthoenstatite (for the linear fit to 573 K in this study) does not compare well with simple elasticity systematics discussed in previous works. Specifically, Duffy and Anderson (1989) estimate that $(dK_S/dT)_P = -12.0 \text{ MPa/K}$ for orthoenstatite. This estimated value does not seem to be relevant, however, to orthoenstatite. Therefore, the strong temperature dependence of the elastic quantities in orthoenstatite observed in this study and in Frisillo and Barsch (1972) should be considered when modeling Earth's shallow upper mantle.

It is suggested from high-pressure room-temperature ultrasonic measurements that $\text{Mg}_2\text{Si}_2\text{O}_6$ orthoenstatite undergoes a high-pressure structural phase transition that is accompanied by acoustic mode-softening between about 9 GPa and 14 GPa (pressures equivalent to $\sim 300 \text{ km}$ depth) (Kung et al., 2004); however, the structure of the high-pressure phase could not be identified in their study. In order to realistically model Earth's upper mantle, future single-crystal elasticity measurements on iron-bearing orthoenstatite at simultaneous high temperature and pressure would be necessary to understand the proposed anomalous elasticity associated with these phase transformations. If the high-temperature high-pressure phase transformation of iron-bearing orthoenstatite to high-clinoenstatite involves significant acoustic mode-softening, a low velocity zone would result around 300 km depth. This would support a solid-state mechanism for seismically observed low-velocity zones in Earth's upper mantle (Stixrude and Lithgow-Bertelloni, 2005).

In Fig. 7, we plot the ratio of the aggregate compressional wave velocity to shear wave velocity (V_P/V_S) as a function of temperature for several minerals in Earth's upper mantle. We find that almost all minerals exhibit a positive temperature derivative of the V_P/V_S ratio, with the exception of orthoenstatite. We also plot V_P/V_S values for orthoenstatite in the crystallographic c -direction [001], which shows the largest acoustic mode-softening (Jackson et al. (2004); listed here in Table 5). In this crystallographic direction, values were obtained up to 1448 K (Jackson et al., 2004).

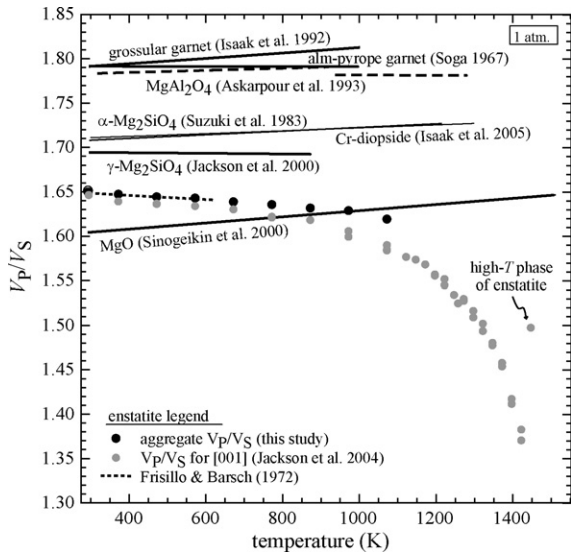


Fig. 7. Experimental determinations of the ratio of aggregate VRH compressional wave velocity and shear wave velocity (V_p/V_s) as a function of temperature (K) for several minerals (close to the Mg end-member) in Earth's mantle. Labels are adjacent to their respective lines; a dashed line is used for $MgAl_2O_4$ because it undergoes an order-disorder transition at 923 K. The solid black spheres represent data from this study for single-crystal natural orthoenstatite with near Mg end-member composition and a dotted line is used for the data from $(Mg_{0.8}Fe_{0.2})_2Si_2O_6$ (Frisillo and Barsch, 1972). The solid gray spheres are data from near Mg end-member orthoenstatite in the crystallographic c -direction [001] that shows the largest observed acoustic mode-softening (from Jackson et al., 2004; listed here in Table 5). Most minerals display a V_p/V_s ratio that increases or is relatively constant with temperature, with the exception of orthoenstatite. Note that the uncertainties for V_p and V_s are typically 1%, therefore the uncertainties in (V_p/V_s) would be approximately, 1.4%.

Orthoenstatite can exhibit very low V_p/V_s ratios, even at moderate temperatures. At temperatures close to the high-temperature ambient pressure structural phase transition of orthoenstatite, V_p/V_s ratios drop to around 1.36, then sharply increase to $V_p/V_s = 1.50$ at 1448 K, the temperature just above where the structural phase transition has occurred (Table 5 and Fig. 7). Therefore, any seismically observed V_p/V_s ratio that decreases with depth could be indicative of an enrichment of orthopyroxene. Also, recent seismic observations in shallow flat-slab subduction areas show very low V_p/V_s ratios (Wagner et al., 2006). These observations could be explained by the presence of high concentrations of orthopyroxene (Wagner et al., 2006).

Acknowledgments

We thank George R. Rossman (California Institute of Technology) for providing the gem quality orthoen-

statite crystals (GRR 649, AMNH 100634). We would also like to thank Michael Carpenter, Ross Angel, Jennifer Kung, Dmitry L. Lakshantov, Don Isaak, Wolfgang Sturhahn, and Lara Wagner for helpful discussions. We acknowledge support of NSF-EAR 0003383 to JDB.

References

- Angel, R.J., Hugh-Jones, D.A., 1994. Equations of state and thermodynamic properties of enstatite pyroxenes. *J. Geophys. Res.* 99, 19777–19783.
- Angel, R.J., Jackson, J.M., 2002. Elasticity and equation of state of orthoenstatite, $MgSiO_3$. *Am. Mineral.* 87, 558–561.
- Askarpour, V., Manghni, M.H., Fassbender, S., Yoneda, A., 1993. Elasticity of $MgAl_2O_4$ spinel up to 1273 K by Brillouin spectroscopy. *Phys. Chem. Miner.* 19, 511–519.
- Bass, J.D., 1989. Elasticity of grossular and spessartite garnets by Brillouin spectroscopy. *J. Geophys. Res.* 84, 7621–7628.
- Bass, J.D., Anderson, D.L., 1984. Composition of the upper mantle: geophysical tests of two petrological models. *Geophys. Res. Lett.* 11 (3), 237–250.
- Bass, J.D., Weidner, D.J., 1984. Elasticity of single-crystal orthoferrosilite. *J. Geophys. Res.* 89 (B6), 4359–4371.
- Chai, M., Brown, J.M., Slutsky, L.J., 1997. The elastic constants of an aluminous orthopyroxene to 12.5 GPa. *J. Geophys. Res.* 102 (B7), 14779–14785.
- Chen, G., Li, B., Liebermann, R.C., 1996. Selected elastic moduli of single-crystal olivines from ultrasonic experiments to mantle pressures. *Science* 272, 979–980.
- Deer, W.A., Howie, R.A., Zussman, J., 1978. *Single-Chain Silicates: Pyroxenes*. John Wiley and Sons.
- Dietrich, P., Arndt, J., 1982. Effects of pressure and temperature on the physical behavior of mantle-relevant olivine, orthopyroxene and garnet. I. Compressibility, thermal properties and macroscopic Grüneisen parameters. In: Schreyer, W. (Ed.), *High-pressure researches in geoscience*. Schweizerbart's Verlagsbuchhandlung, Stuttgart, pp. 293–306.
- Duffy, T.S., Vaughan, M.T., 1988. Elasticity of enstatite and its relationship to crystal structure. *J. Geophys. Res.* 93 (B1), 383–391.
- Duffy, T.S., Anderson, D.L., 1989. Seismic velocities in mantle minerals and the mineralogy of the upper mantle. *J. Geophys. Res.* 94, 1895–1912.
- Flesch, L.M., Li, B., Liebermann, R., 1998. Sound velocities of polycrystalline $MgSiO_3$ -orthopyroxene to 10 GPa at room temperature. *Am. Mineral.* 83, 444–450.
- Frisillo, A.L., Barsch, G.R., 1972. Measurement of single-crystal elastic constants of bronzite as a function of pressure and temperature. *J. Geophys. Res.* 77, 6360–6384.
- Frisillo, A.L., Buljan, S.T., 1972. Linear thermal expansion coefficients of orthopyroxene to 1000 °C. *J. Geophys. Res.* 77, 7115–7117.
- Hugh-Jones, D., 1997. Thermal expansion of $MgSiO_3$ and $FeSiO_3$ ortho- and clinopyroxenes. *Am. Mineral.* 82, 689–696.
- Hugh-Jones, D.A., Angel, R.J., 1994. A compressional study of $MgSiO_3$ orthoenstatite to 8.5 GPa. *Am. Mineral.* 79, 405–410.
- Isaak, D., Anderson, O.L., Oda, H., 1992. High-temperature thermal expansion and elasticity of calcium-rich garnets. *Phys. Chem. Miner.* 19, 106–120.

- Isaak, D.G., Ohno, I., Lee, P.C., 2006. The elastic constants of monoclinic single-crystal chrome-diopside to 1300 K. *Phys. Chem. Miner.* 32, 691–699.
- Ita, J., Stixrude, L., 1993. Density and elasticity of model upper mantle compositions and their implications for whole mantle structure. In: *Evolution of the Earth and Planets*, Geophysical Monograph 74, vol. 14, IUGG.
- Ito, J., 1975. High temperature solvent growth of orthoenstatite, MgSiO_3 , in air. *Geophys. Res. Lett.* 2, 533–536.
- Jackson, J.M., Sinogeikin, S.V., Bass, J.D., 1999. Elasticity of MgSiO_3 orthoenstatite. *Am. Mineral.* 84, 677–680.
- Jackson, J.M., Sinogeikin, S.V., Bass, J.D., 2000. Sound velocities of $\gamma\text{-Mg}_2\text{SiO}_4$ to 873 K by Brillouin spectroscopy. *Am. Mineral.* 85, 296–303.
- Jackson, J.M., Sinogeikin, S.V., Carpenter, M.A., Bass, J.D., 2004. Novel phase transition in orthoenstatite. *Am. Mineral.* 89, 239–245.
- Jackson, J.M., Palko, J., Andrault, D., Sinogeikin, S.V., Lakshtanov, D.L., Wang, J., Bass, J.D., Zha, C.-S., 2003. Thermal expansion of natural orthoenstatite to 1473 K. *Eur. J. Mineral.* 15, 469–473.
- Jiang, F.M., Speziale, S., Duffy, T.S., 2004. Single-crystal elasticity of grossular- and almandine-rich garnets to 11 GPa by Brillouin scattering. *J. Geophys. Res.* 109 (B10), B10210.
- Kumazawa, M., 1969. The elastic constants of single-crystal orthopyroxene. *J. Geophys. Res.* 74 (25), 5973–5980.
- Kung, J., Li, B., Uchida, T., Wang, Y., Neuville, D., Liebermann, R.C., 2004. In situ measurements of sound velocities and densities across the orthopyroxene—high-pressures clinopyroxene transition in MgSiO_3 at high pressure. *Phys. Earth Planet. Interiors* 147, 27–44.
- Kurat, G., Palme, H., Embey-Isztin, A., Touret, J., Ntaflos, T., Spettel, B., Brandstatter, F., Palme, C., Dreibus, G., Prinz, M., 1993. Petrology and geochemistry of peridotites and associated vein rocks of Zabargad Island, Red Sea, Egypt. *Mineral. Petrol.* 48, 309–341.
- Li, B., Liebermann, R.C., Weidner, D.J., 1998. Elastic moduli of wadsleyite ($\beta\text{-Mg}_2\text{SiO}_4$) to 7 Gigapascals and 873 Kelvin. *Science* 281, 675–677.
- Miyake, A., Kawano, J., 2005. Molecular dynamics simulations of MgSiO_3 enstatite and seismic discontinuity in the upper mantle. *Geophys. Res. Lett.* 32, L13310, doi:10.1029/2004GL022264.
- Musgrave, M.J.P., 1970. *Crystal Acoustics: Introduction to the Study of Elastic Waves and Vibrations in Crystals*. Holden-Day Inc., San Francisco.
- Nestola, F., Diego Gatta, G., Boffa Ballaran, T., 2006. The effect of Ca substitution on the elastic and structural behavior of orthoenstatite. *Am. Mineral.* 91, 809–815.
- Pacalo, R.E.G., Weidner, D.J., 1997. Elasticity of majorite, MgSiO_3 tetragonal garnet. *Phys. Earth Planet. Interiors* 99, 145–154.
- Parise, J.B., Wang, Y., Gwanmesia, G.D., Zhang, J., Sinelnikov, Y., Chmielowski, J., Weidner, D.J., Liebermann, R.C., 1996. The symmetry of garnets on the pyrope ($\text{Mg}_3\text{Al}_2\text{Si}_3\text{O}_{12}$)—majorite (MgSiO_3) join. *Geophys. Res. Lett.* 23, 3799–3802.
- Ringwood, A.E., 1991. Phase transformations and their bearing on the constitution and dynamics of the mantle. *Geochim. Cosmochim. Acta* 55, 2083–2110.
- Sandercock, J.R., 1982. Trends in Brillouin scattering: studies of opaque materials, supported films, and central modes, in topics in applied physics. In: Cardona, M., Guntherodt, G. (Eds.), *Light Scattering in Solids III: Recent Results*. Springer-Verlag, Berlin.
- Sinogeikin, S.V., Bass, J.D., 2000. Single-crystal elasticity of pyrope and MgO to 20 GPa by Brillouin scattering the diamond cell. *Phys. Earth Planet. Interiors* 120, 43–62.
- Sinogeikin, S.V., Bass, J.D., 2002a. Elasticity of majorite and a majorite-pyrope solid solution to high pressure: implications for the transition zone. *Geophys. Res. Lett.* 29 (2), 1017.
- Sinogeikin, S.V., Bass, J.D., 2002b. Elasticity of pyrope and majorite-pyrope solid solutions to high temperatures. *Earth Planet. Sci. Lett.* 203, 549–555.
- Sinogeikin, S.V., Jackson, J.M., O'Neill, B., Palko, J., Bass, J.D., 2000. Compact high-temperature cell for Brillouin scattering measurements. *Rev. Sci. Instrum.* 71, 201–206.
- Sinogeikin, S.V., Katsura, T., Bass, J.D., 1998. Sound velocities and elastic properties of Fe-bearing wadsleyite and ringwoodite. *J. Geophys. Res.* 103 (B9), 20819–20825.
- Skogby, H., Bell, D.R., Rossman, G.R., 1990. Hydroxide in pyroxene: variations in the natural environment. *Am. Mineral.* 75, 764–774.
- Smyth, J.R., 1974a. Experimental study of the polymorphism of enstatite. *Am. Mineral.* 59, 345–352.
- Smyth, J.R., 1974b. The high temperature crystal chemistry of clinohypersthene. *Am. Mineral.* 59, 1069–1082.
- Soga, N., 1967. Elastic constants of garnet under pressure and temperature. *J. Geophys. Res.* 72 (16), 4227–4234.
- Stixrude, L., Lithgow-Bertelloni, C., 2005. Mineralogy and elasticity of the oceanic upper mantle: origin of low velocity zone. *J. Geophys. Res.* 110, B03204, doi:10.1029/2004JB002965.
- Suzuki, I., Anderson, O., 1983. Elasticity and thermal expansion of a natural garnet up to 1000 K. *J. Phys. Earth* 31, 125–138.
- Suzuki, I., Anderson, O.L., Sumino, Y., 1983. Elastic properties of a single-crystal forsterite Mg_2SiO_4 , up to 1200 K. *Phys. Chem. Miner.* 10, 38–46.
- Takahashi, E., Ito, E., 1987. Mineralogy of mantle peridotite along a model geotherm up to 700 km depth. In: Manghnani, M.H., Syono, Y. (Eds.), *High-Pressure Research in Mineral Physics*. AGU, Washington, pp. 427–437.
- Vaughan, M.T., Bass, J.D., 1983. Single crystal elastic properties of protoenstatite: a comparison with orthoenstatite. *Phys. Chem. Miner.* 10, 62–68.
- Wagner, L., Beck, S., George, Z., Ducea, M., 2006. Depleted lithosphere, cold, trapped asthenosphere, and frozen melt puddles above the flat slab in central Chile and Argentina. *Earth Planet. Sci. Lett.* 245, 289–301.
- Webb, S.L., Jackson, I., 1993. The pressure dependence of the elastic moduli of single-crystal orthopyroxene. *Eur. J. Mineral.* 5, 1111–1119.
- Weidner, D.J., Carleton, H.R., 1977. Elasticity of coesite. *J. Geophys. Res.* 82, 1334–1346.
- Weidner, D.J., Bass, J.D., Vaughan, M.T., 1982. The effect of crystal structure and composition on elastic properties of silicates. In: Akimoto, S., Manghnani, M. (Eds.), *High Pressure Research in Geophysics*. Center for Academic Publication Japan, Tokyo.
- Weidner, D.J., Vaughan, M.T., 1982. Elasticity of pyroxenes: effects of composition versus crystal structure. *J. Geophys. Res.* 87 (B11), 9349–9353.
- Weidner, D.J., Wang, H., Ito, J., 1978. Elasticity of orthoenstatite. *Phys. Earth Planet. Interiors* 17, 7–13.
- Whitfield, C.H., Brody, E.M., Bassett, W.A., 1976. Elastic moduli of NaCl by Brillouin scattering at high pressure in a diamond anvil cell. *Rev. Sci. Instrum.* 47, 942–947.
- Winter, J.D., 2001. *An Introduction to Igneous and Metamorphic Petrology*. Prentice-Hall Inc., New Jersey.
- Yang, H., Ghose, S., 1994. Thermal expansion, Debye temperature and Grüneisen parameters of synthetic (Fe,Mg) SiO_3 orthopyroxenes. *Phys. Chem. Miner.* 20, 575–586.

- Yang, H., Ghose, S., 1995a. High temperature single crystal X-ray diffraction studies of the ortho-proto phase transition in enstatite, $\text{Mg}_2\text{Si}_2\text{O}_6$ at 1360 K. *Phys. Chem. Miner.* 22, 300–310.
- Yang, H., Ghose, S., 1995b. A transitional structural state and anomalous Fe-Mg order-disorder in Mg-rich orthopyroxene, $(\text{Mg}_{0.75}\text{Fe}_{0.25})\text{Si}_2\text{O}_6$. *Am. Mineral.* 80, 9–20.
- Zha, C.-S., Duffy, T.S., Downs, R.T., Mao, H.-K., Hemley, R.J., 1996. Sound velocity and elasticity of single-crystal forsterite to 16 GPa. *J. Geophys. Res.* 101, 17535–17545.
- Zhao, Y., Schiferl, D., Shankland, T.J., 1995. A high P - T single-crystal X-ray diffraction study of thermoelasticity of MgSiO_3 orthoenstatite. *Phys. Chem. Miner.* 22, 393–398.